Pure Reduced Polyoxometalates Materials as Electroactive Materials Toward Proton Energy Storage Device

Chen Wang[a], Wen-Hang Guo[b], Wen Tang[a], Yun-Zuo Cui[b], Zhao-Peng Qi[a*], Song Liang[d*], Hong-Ying Zang[b*], Zhong-Min Su[c]

[a] *School of Chemistry and Chemical Engineering, Key Laboratory of Inorganic Functional Materials, Huangshan University, Huangshan 245042, P. R. China*

[b] *Key Laboratory of Polyoxometalate and Reticular Material Chemistry of Ministry of Education at Universities of Jilin Province, Faculty of Chemistry, Northeast Normal University, Changchun 130024, P. R. China*

[c] *State Key Laboratory of Supramolecular Structure and Materials, Institute of Theoretical Chemistry, College of Chemistry, Jilin University, Changchun 130021, P. R. China*

[d] *Key Laboratory of Bionic Engineering of the Ministry of Education, College of Biological and Agricultural Engineering, Jilin University, Changchun, 130012 P. R. China*

Materials and General Methods

All reagents are purchased from Aladin, and used without further purification.

The FT-IR spectra were taken on a Varian FT-IR 640 spectrometer (KBr pellets) in the range of 400-4000 cm^{-1}. Powder X-ray diffraction (PXRD) patterns were analyzed on a Rigaku D-max 2550 instrument using Cu Kα (λ = 1.5406 Å) radiation. X-ray photoelectron spectroscopy (XPS) was performed on a Thermo ESCALAB 250 instrument. The morphology of complexes was analyzed by scanning electron microscopy (SEM, Hitachi SU-70). A CHI760 electrochemical workstation was used to measure electrochemical capability and collect data. The classical three-electrode system was adopted, in which the saturated calomel electrode (SCE) was used as reference electrode and the Pt wire as the counter electrode.

Preparation of Complexes 1-2

Synthesis of Complex 1

$H_{10}\{Cu^{II}_{0.5}[Mo^{V}_{6}O_{12}(OH)_3(HPO_4)_4]_2\}_2\cdot 8HPy\cdot 24H_2O$ (**1**)

0.195 g (1.14 mmol) $CuCl_2\cdot 2H_2O$, 0.2 g (0.83 mmol) $Na_2MoO_4\cdot 2H_2O$, 50 mg (0.48 mmol) $N_2H_4\cdot HCl$, 1 mL H_3PO_4 and 1 mL pyridine are added in 6 mL deionized water. And then stirring at room temperature for 30 minutes, transfer to a reaction kettle and placing in an oven at 150 ℃ for 3 days, and cooling to temperature to obtain a red block crystal. Yield:

31%.

Synthesis of Complex 2

$H_8Cd^{II}[Mo^{V}_6O_{12}(OH)_3(HPO_4)_4]_2 \cdot 2Cl \cdot 2HPy \cdot 2Me_2NH$ (**2**)

0.29 g (1.44 mmol) $CdCl_2 \cdot H_2O$, 0.49 g (2.03 mmol) $Na_2MoO_4 \cdot 2H_2O$, 2 mL H_3PO_4 and 2 mL pyridine are added in 6 mL deionized water and 1 mL N,N-Dimethyl Formamide. And then stirring at room temperature for 30 minutes, transfer to a reaction kettle and placing in an oven at 150 ℃ for 3 days, and cooling to temperature to obtain a red block crystal. Yield: 39%.

Preparation of working electrodes of complexes

The complexes, Ketjen black and PVDF (polyvinylidene fluoride) were mixed in a certain mass ratio (1:1:1), and then N-methylpyrrolidone was added to form a paste. The paste was ground about 5 mins, which was coated on the surface of carbon paper. After the electrode was dried at 60 ℃ overnight, its mass change was measured, and the mass loading of active material was determined to be 1 mg.

Preparation of n-CP@PANI electrodes

The electrochemical deposition method was used to prepare **n**-CP@PANI electrodes. The detailed experimental steps are as follows[S1]: the **n**-CP electrodes were acted as working electrode in a three-electrodes system (saturated calomel electrode as reference and Pt wire as counter). The

electrolyte was prepared by mixing 50 mL water, 1.2 mL aniline and 2.1 mL concentrated HCl. The electro-deposition experiments were conducted during a potential window between -0.2 - +1.0 V for one cycle, then the samples were dried at 60℃ for 12h.

Preparation of PVA-based hydrogel electrolytes

The PVA-based hydrogel electrolytes are prepared as follows [S2]: 2 g PVA solution and 0.1 g glycerol were added into a clean glass vial, and 0.4 g H_2SO_4 were added, followed by stirred at room temperature for 12 hours to obtain a homogeneous solution. After that, 2 μL 25 wt% glutaraldehyde was added into the above solution and stirred for 1 min.

Preparation of rechargeable devices

The newly prepared PVA-based hydrogel electrolyte was dropped on two **n**-CP@PANI electrodes, which was dried at room temperature. And then, two **n**-CP@PANI electrodes were affixed together and hot-pressed at 50℃ for 10 mins. The formed devices were placed in a closed container with saturated potassium sulfate about 3 hours

Proton conductivity characterization

Firstly, the power of Complexes was poured into a mold with an inner diameter of 10 mm and applied a pressure of 2 MPa to obtain a sheet-like sample. Clamp the sheet-like sample between two gold-plated electrodes amd place it in the Stanwood SC-80-CC-3 constant temperature and

humidity chamber to control the relative humidity and temperature of the testing environment. The proton conductivity was measured using an alternating Solatron SI 1260 impedance/gain phase current (AC) impedance analyzer with a frequency range of 1 Hz to 1 MHz and an applied voltage of 100mV. Zview software is used to fit impedance data and calculate conductivity (σ) based on resistance value (R), with a value of σ = d/RA (eq. s1). Among them, d is the thickness of the sheet-like sample, R is the resistance value, and A is the area of the sheet-like sample. The activation energy is calculated using the Arrhenius equation,

$$\sigma_T=\sigma_0 \exp(-E_a/k_BT) \qquad \text{(eq. s1)}$$

σ_0 is the pre exponential factor, T is the temperature, and k_B is the Boltzmann constant

The specific capacity value, areal capacitance, energy density and corresponding power density can be calculated from the equations [S4]:

$$\text{Specific capacity} = \frac{2I \times \triangle t}{m \times \triangle V} \qquad \text{(eq. s2)}$$

$$\text{Areal capacitance} = \frac{2I \times \triangle t}{s \times \triangle V} \qquad \text{(eq. s3)}$$

$$\text{Energy density} = CV^2/2 \qquad \text{(eq. s4)}$$

$$\text{Power density} = 3600E/t \qquad \text{(eq. s5)}$$

Where I (A) is discharge current, ΔV (V) is potential change, m (g) is the amount of active material, s (cm^{-2}) is the area of electrode, Δt (s) is discharging time, E (Wh/kg or Wh/g) is energy density, P (W/kg or W/g) is power density.

X-Ray crystallography study

A Bruker SMART APEX II with Mo-*Kα* radiation (λ = 0.71073 Å) was used to collect X-Ray diffraction analyses data by using ω and θ scan mode at 293 K. The detailed crystal data and structure refinement for **Complexes 1**-**2** is shown in Table S1. Selected bond lengths and angles are listed in Table S2. Crystallographic data for the compounds reported in this work have been deposited in the Cambridge Crystallographic Data Center with CCDC numbers 2204880 and 2519566 for **Complexes 1**-**2**.

Figure

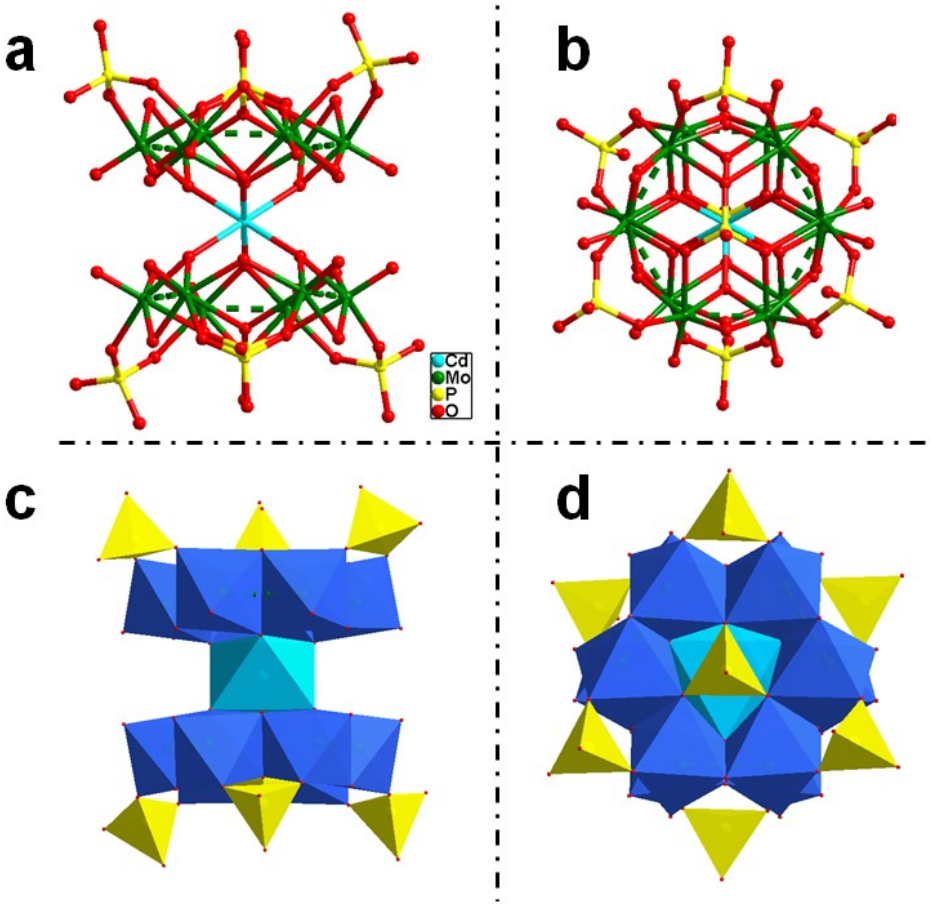

Figure S1. (a-b) The structure of $\{P_4Mo^V_6O_{31}\}$ anions from different views (top views and side views); (c-d) The polymer model of $\{P_4Mo^V_6O_{31}\}$ anions from different views (top views and side views).

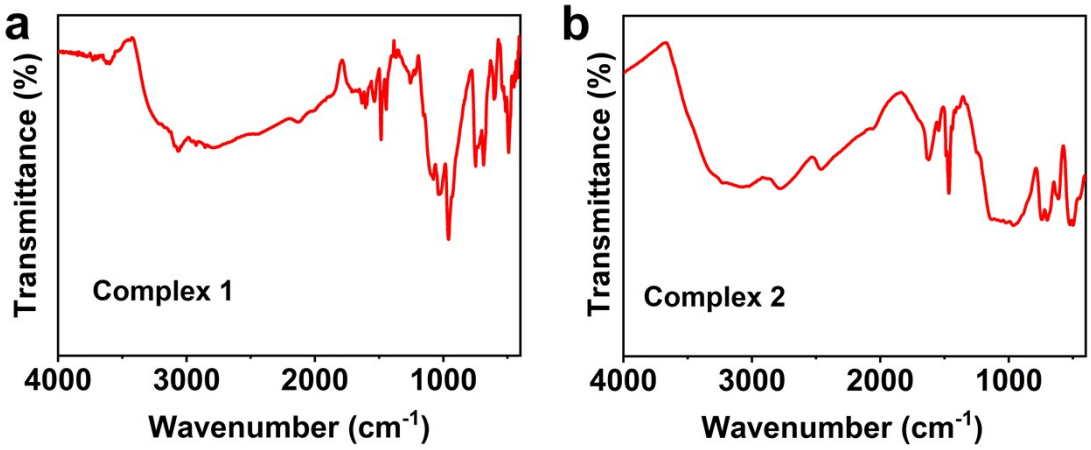

Figure S2. The FT-IR spectra of complexes **1**-**2**.

For complex **1**, the peaks at 494 cm^{-1} and 748 cm^{-1} are attributed to *v*(Mo-O-Mo) bonds, the peaks at 957 cm^{-1} and 1039 cm^{-1} are attributed to *v*(Mo=O), *v*(P-O) bonds.

For complex **2**, the peaks at 496 cm^{-1} and 743 cm^{-1} are attributed to *v*(Mo-O-Mo) bonds, the peaks at 960 cm^{-1} and 1024 cm^{-1} are attributed to *v*(Mo=O), *v*(P-O) bonds. [S3-S4]

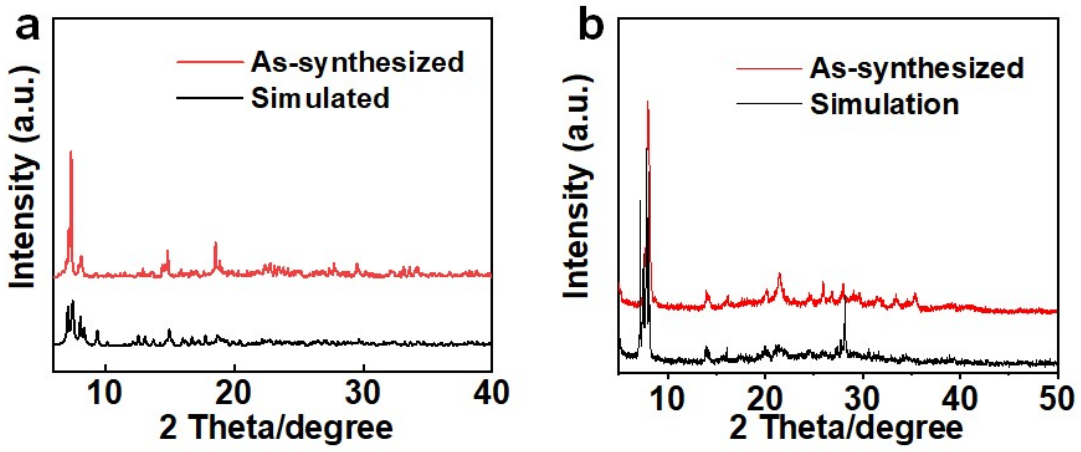

Figure S3. The Powder X-ray diffraction patterns of complexes **1**-**2**.

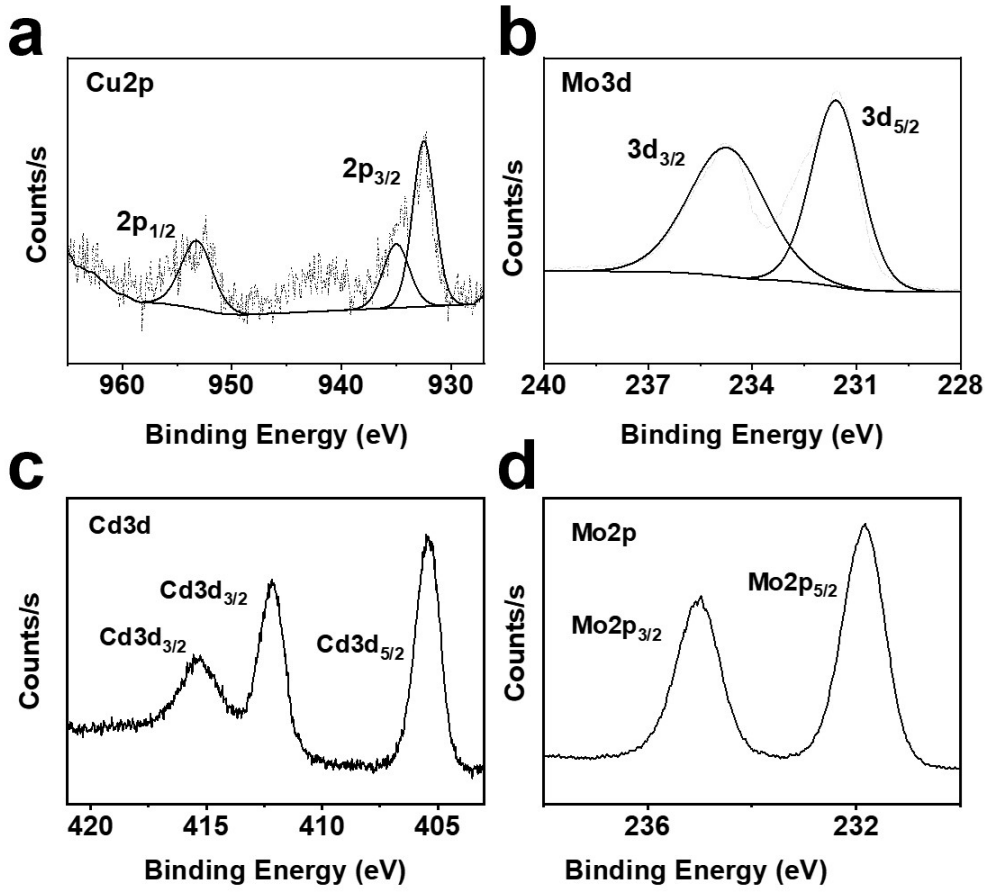

Figure S4. The X-Ray photoelectron spectroscopy of complexes **1**-**2**.

As shown in Figure S4, the binding energies of $Cu2p_{1/2}$ and $Cu2p_{3/2}$ are 953.06 eV and 932.97 eV, indicating that the valence states of all Cu atoms in complex **1** are +2 [S5]. For $Mo3d_{3/2}$ and $Mo3d_{5/2}$, the binding energies are located at 235.27 eV and 232.17 eV, indicating that the valence states of all Mo atoms in complex **1** are +5 [S6].

The binding energies of $Cd3d_{3/2}$, $Cd3d_{3/2}$ and $Cd3d_{5/2}$ are 415.35 eV, 412.16 eV and 405.51 eV, indicating that the valence states of all Cd atoms in complex **2** are +2 [S7]. For $Mo3d_{3/2}$ and $Mo3d_{5/2}$, the binding energies are located at 234.97 eV and 231.82 eV, indicating that the valence states of all Mo atoms in complex **2** are +5.

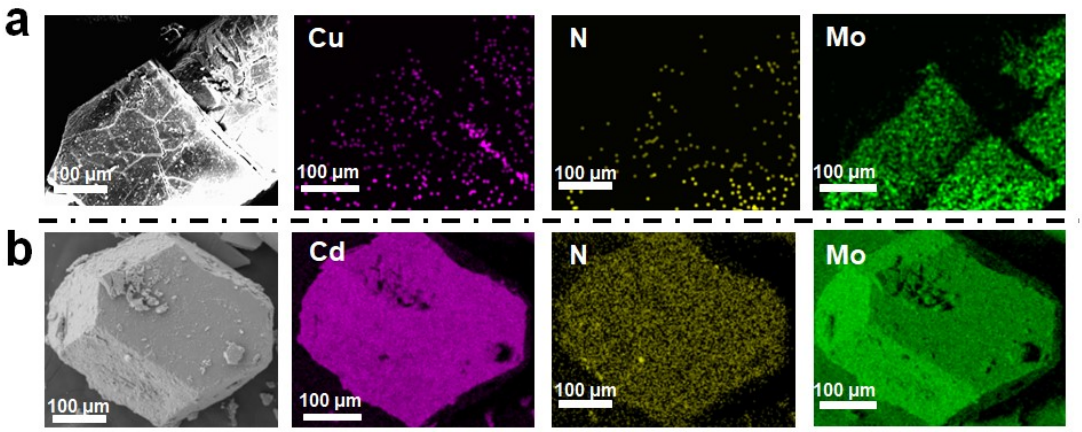

Figure S5. SEM and EDS elemental mapping images of complexes **1**-**2**.

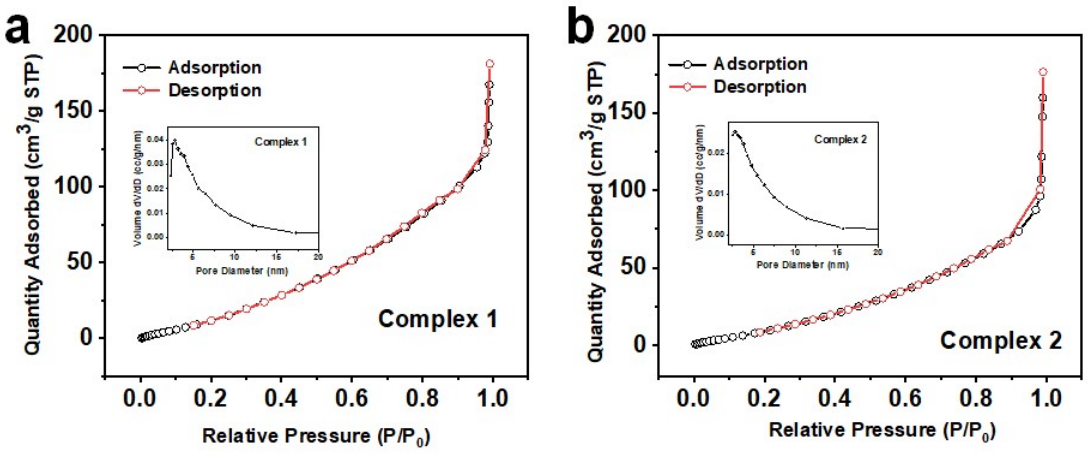

Figure S6. The BET surface area and pore size distribution analyses of complexes **1**-**2**.

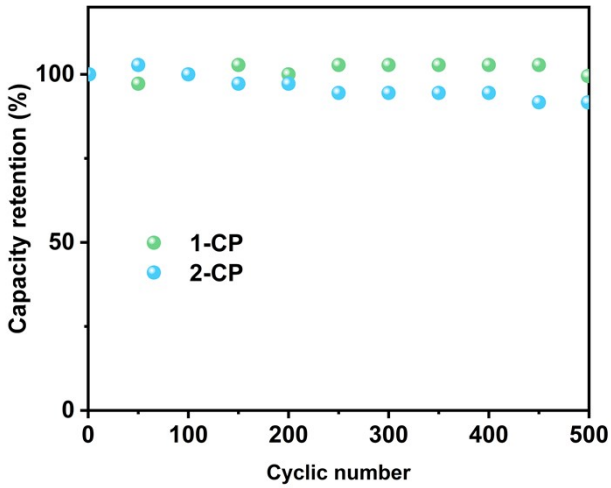

Figure S7. Capacity retention of **n**-CPs in 500 charge-discharge cycles (three-electrodes system in H_2SO_4 electrolyte).

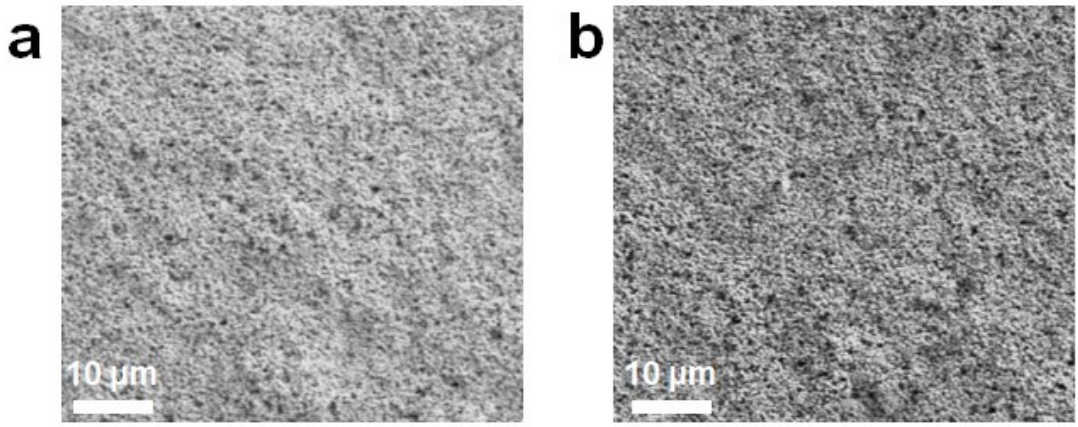

Figure S8. (a)(b) The SEM images of complexes-modified electrodes with large scale. (Scale: 10 μm).

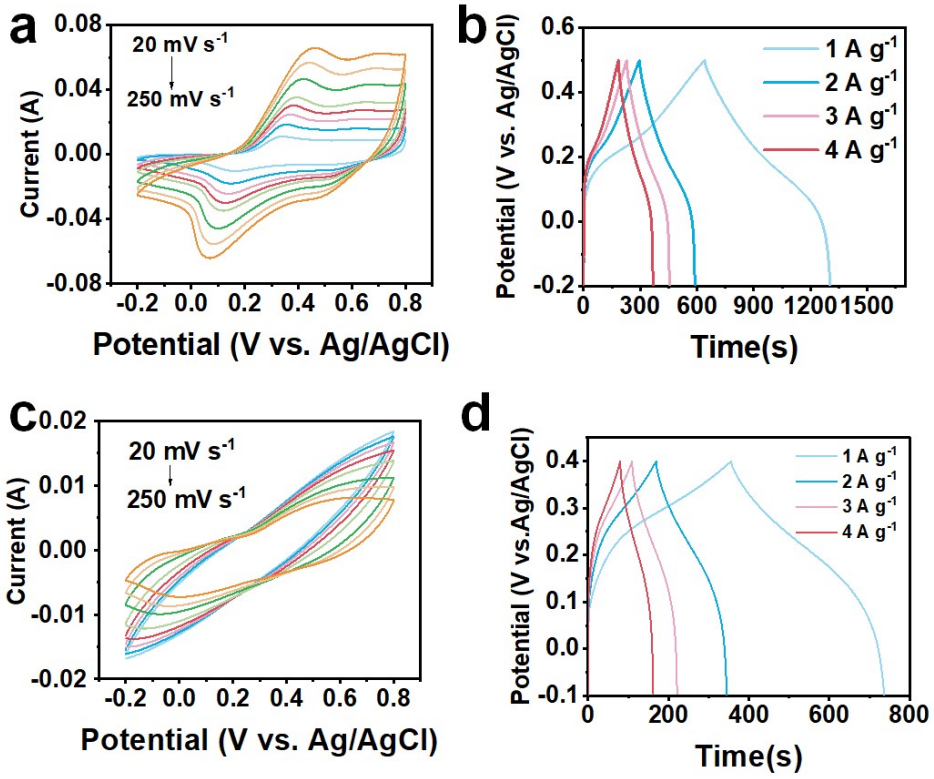

Figure S9. (a) The CV curves of **1**-CP@PANI with scan rates from 20 mV s^{-1} to 250 mV s^{-1}; (b) The GCD curves of **1**-CP@PANI with current densities from 1 A g^{-1} to 4 A g^{-1}; (c) The CV curves of **2**-CP@PANI with scan rates from 20 mV s^{-1} to 250 mV s^{-1}; (d) The GCD curves of **2**-CP@PANI with current densities from 1 A g^{-1} to 4 A g^{-1}.

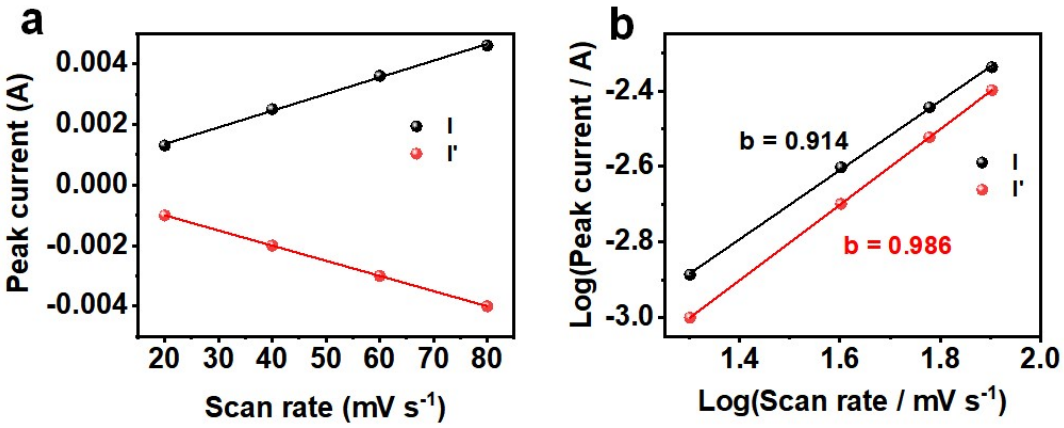

Figure S10. (a) Linear relationship between peak current and scan rates; (b) Logarithmic diagram of peak current and scan rates.

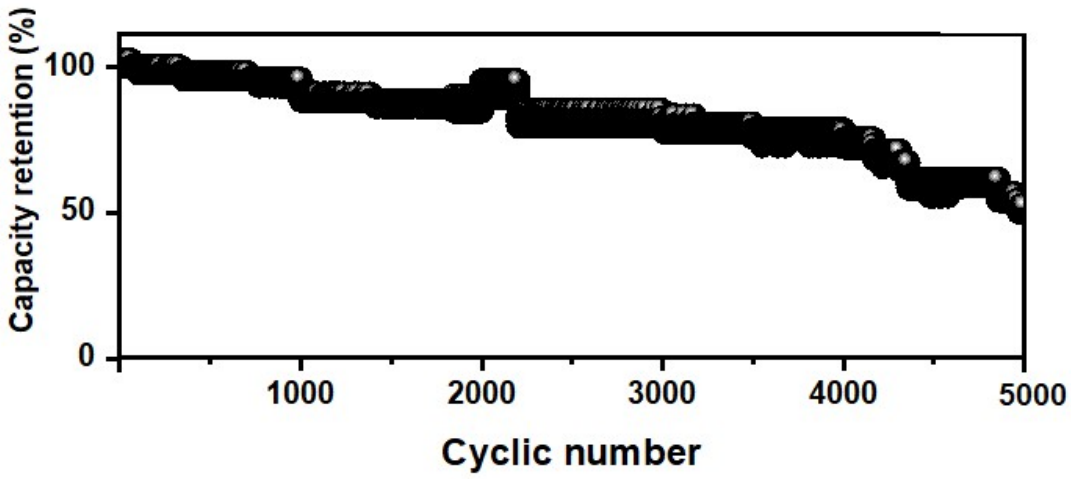

Figure S11. Capacity retention and Columbic efficiency in 5000 charge-discharge cycles.

Table S1. Crystal Data and Structure Refinement for Complexes

	Complex 1	**Complex 2**
formula	$C_{40}H_{80}CuN_8O_{131}P_{16}Mo_{24}$	$C_{14}H_{40}CdO_{62}P_8Mo_{12}Cl_2$
*F*w	5630.74	2838.87
crystal system	Triclinic	Triclinic
space group	*P -1*	*P -1*
a (Å)	15.7897(11)	13.298(2)
b (Å)	16.1670(12)	13.314(2)
c (Å)	17.5673(14)	15.723(3)
α (°)	89.382(4)	112.498(7)
β (°)	82.620(4)	103.961(7)
γ (°)	82.968(6)	103.425(7)
V (Å^3)	4413.8(6)	2326.7(7)
Z	1	1
D_c (g·cm^{-3})	2.118	2.029
μ (mm^{-1})	2.009	2.067
F(000)	2701	1358
R_1[a] [I > 2σ(I)]	0.0449	0.0306
wR_2[b] (all data)	0.1218	0.0832
GOF on F^2	1.069	1.068

[a] $R^1 = \Sigma||F_o|-|F_c||/\Sigma|F_o|$; [b] $wR^2 = [\Sigma w(F_o^2-F_c^2)^2/\Sigma w(F_o^2)^2]^{1/2}$, $w = [\sigma^2(F_o^2)+(AP)^2+BP]^{-1}$.

Table S2. Selected bond distances(Å) and angles (°) for Complexes

Complex 1			
Cu(1)-O(57)	2.298(5)	Cu(1)-O(48)	2.300(6)
Cu(2)-O(28)	2.297(5)	Cu(2)-O(24)#1	2.317(5)
Cu(2)-O(30)	2.292(5)	P(2)-O(49)	1.515(7)
P(2)-O(51)	1.508(7)	P(6)-O(12)	1.543(8)
Cu(1)-O(43) #2	2.336(6)	P(6)-O(14)	1.551(7)
P(8)-O(4)	1.491(7)	P(8)-O(1)	1.539(7)
O(28)-Cu(2)-O(24)	95.33(19)	O(30)-Cu(2)-O(28)	96.47(19)
O(30)-Cu(2)-O(24)	96.6(2)	O(48)-Cu(1)-O(43)	97.0(2)
O(57)-Cu(1)-O(43)	96.45(19)	O(57)-Cu(1)-O(48)	96.62(19)
Symmetry codes**:** #1 -X, 1-Y, Z; #2 1-X, -Y, 1-Z			
Complex 2			
Cd(1)-O(9)	2.315(6)	Cd(1)-O(8)	2.271(4)
Cd(1)-O(19)	2.269(7)	Mo(5)-O(9)	1.973(8)
Mo(6)-O(7)	1.678(5)	Mo(1)-O(30)	3.275(6)
P(1)-O(29)	1.507(8)	P(4)-O(3)	1.528(9)
O(8)-Cd(1)-O(19)	95.81(11)	O(8)-Cd(1)-O(9)	97.08(18)
O(9)-Cd(1)-O(19)	96.16(7)	Mo(1)-O(6)-Mo(6)	113.23(15)

Table S3. Comparison of proton conductivity with reported POMs-based materials

Materials	**Proton conductivity (mS cm^{-1})**	**Ref.**
$[Zr(tarH)WO_2]^{48+}$	3.82	Rare Metals., 2024, 44, 1401.
PMoZn-2	6.65	Inorg. Chem. Commun., 2023, 155, 111053.
$\{Co_8(PO_3)_4(TeMo_6O_{21})_6\}$	11.1	Chin. Chem. Lett., 2025, 10.1016/j.cclet.2025.111413.
$Cs_8K_2Na_2H_4\{[(C_6H_6)Ru]_6Mo_{24}O_{86}\}\cdot 35H_2O$	12	Inorg. Chem., 2024, 63, 22464.
$[PMo_8^{V}Mo_4^{VI}O_{34}(OH)_6Zn_4][LO]$	2.66	Inorg. Chem., 2023, 62, 5565.
$Na_{16}(H_3O)_4[H_2N(CH_3)_2]_2[As_{12}Mo_{31}O_{129}Rh_4(OH)_2(H_2O)]\cdot 27H_2O$	9.1	Inorg. Chem., 2025, 64, 21849.

$Na_6H_{14}[Mo^{VI}_{84}Mo^{V}_{24}O_{306}(OH)32]\cdot 130H_2O$	5.14	Inorg. Chem., 2025, 64, 15470.
CUST-834	3.63	ACS Materials Lett., 2025, 7, 3588.
$(NH_4)_3[AlMo_6O_{24}H_6]\cdot 7H_2O$	0.206	Inorg. Chem., 2025, 64, 19933.
$H_4[TEDA][\delta\text{-}Mo_8O_{26}]\cdot 3H_2O$	0.418	New J. Chem., 2018, 42, 16516.
Complex **1**	9.63	**This work**
Complex **2**	2.21	**This work**

Table S4. Comparison of capacity retention with other solid-state capacitors

Solid-state capacitor	**Cyclic number**	**Capacity retention**	**Ref.**
Zn||AC supercapacitor	2500	36.4%	Adv. Maters., 2024, 36, 2400099.
HEF	1000	73.2%	Chem. Eng. J., 2022, 439, 135741.
PANI-ZIF-67-CC	2000	80%	J. Am. Chem. Soc., 2015, 137, 4920.
NAM−EDAG	1100	54.5%	ACS Nano., 2016, 10, 5304.
PANI-PMo_{12}&PW_{12}/PVA	400	90%	CCS Chem, 2020, 2, 1649.
2@PANI-2-SC	1000	61.37%	Inorg. Chem. Front., 2023,10, 3641.
1-CP@PANI-SC	1000	94.2%	**This work**
1-CP@PANI-SC	5000	52.3%	**This work**

Table S5. Comparison of specific capacitance with other POMs-based solid-state capacitors

Solid-state capacitor	**Specific capacitance**	**Ref.**
1-CC@PANI-SC	312.47 F g^{-1}	Electron., 2025, 3, e70019
1@PANI-1-SCs	209.4 F g^{-1}	Inorg. Chem. Front., 2023,10, 3641.
2@PANI-1-SCs	127.1 F g^{-1}	Inorg. Chem. Front., 2023,10, 3641.
PANI-PMo_{12}&PW_{12}-SCs	7.69 F/cm^2	CCS Chem, 2020, 2, 1649.
in sit-MOF1@PANI-PMo_{12}&PW_{12} SC	265.55 mAh g^{-1}	Adv. Funct. Maters., 2025, 35(15), 2419752.
in sit-MOF2@PANI-PMo_{12}&PW_{12} SC	366.94 mAh g^{-1}	Adv. Funct. Maters., 2025, 35(15), 2419752.
1-CP@PANI-SC	330.12 F g^{-1}	**This work**

Table S6. Comparison of energy density and power density with other solid-state capacitors

Solid-state capacitor	**Energy density (Wh kg^{-1})**	**Power density (W kg^{-1})**	**Ref.**
PANI-Mn	37	368	Adv. Electron. Mater., 2019, 5, 1900816.
NPCNFs	28.06	250	J. Mater. Chem. A., 2016, 4, 4180.
Functionalized Carbon Cloth	9.2	250	Electrochim. Acta, 2012, 64, 17.
D/QD/DMP	29.4	398	ACS Appl. Energy Mater., 2019, 2, 6642.
PPy-coated CNTs/quasi-solid electrolyte	51.38	850	Adv. Sci., 2020, 7, 2000587.
rGO/PANI	9.2	1000	J. Power Sources., 2017, 342, 1.

References

[S1] C. M. Zhu, Y. He, Y. J. Liu, et al. ZnO@MOF@PANI core-shell nanoarrays on carbon cloth for high-performance supercapacitor electrodes, J. Energy Chem., 2019, 35, 124.

[S2] D. M. Cheng, B. Li, S. Sun, et al. Proton-Conducting Polyoxometalates as Redox Electrolytes Synergistically Boosting the Performance of Self-Healing Solid-State Supercapacitors with Polyaniline, CCS Chem., 2021, 3, 1649.

[S3] Y. J. Li, C. X. Li, S. B. Zhou, et al. Two-Dimensional Layer $\{P_4Mo_6\}$ Clusters Constructed with N-Ligands for Bifunctional Properties of Proton Conduction and Supercapacitors, Inorg. Chem., 2025, 64, 443.

[S4] C. Wang, Z. X. Gao, H. Y. Zang, et al. Solid-State Supercapacitors Based On Polyoxometalate-Based Crystalline Materials Modified with Polyaniline, Inorg. Chem. Front., 2023, 10, 3641.

[S5] Jo M, Tanaka A. Auger electron peaks of Cu in XPS, Appl. Surf. Sci., 1996, 100, 11.

[S6] X. J. Zhang, Y. Y. Ma, H. X. Bi, et al. Wheel-shaped molybdenum(V) cobalt-phosphate cluster as a highly sensitive bifunctional photoelectrochemical sensor for the trace determination of Cr(VI) and tetracycline, Inorg. Chem. Front., 2022, 9, 6457.

[S7] R. Ospina, S. A. Rincón-Ortiz. Cadmium selenide by XPS, Surf. Sci.

Spectra, 2020, 27(1), 014021.